ChemPubSoc Europe
DOI: 10.1002/cssc.201500349
Full Papers

Electron Bottleneck in the Charge/Discharge Mechanism of Lithium Titanates for Batteries

Edgar Ventosa,*[a] Marcel Skoumal,[a] Francisco Javier Vazquez,[a] Cristina Flox,[a] Jordi Arbiol,[c] and Joan Ramon Morante[a, b]

The semi-solid flow battery (SSFB) is a promising storage energy technology featured by employing semi-solid fluid electrodes containing conductive additive and active Li-ion battery materials. The state of art anode material for SSFB is $Li_4Ti_5O_{12}$ (LTO). This work shows that LTO improves drastically the performance in fluid electrode via hydrogen annealing manifesting the importance of the electrical conductivity of the active material in SSFBs. On the other hand, the properties of fluid electrodes allow the contributions of ionic and electrical resistance to be separated in operando. The asymmetric overpotential observed in $Li_4Ti_5O_{12}$ and TiO_2 is proposed to originate from the so-called electron bottleneck mechanism based on the transformation from electrically insulator to conductor upon (de-)lithiation, or vice versa, which should be considered when modelling, evaluating or designing advanced materials based on $Li_4Ti_5O_{12}$, TiO_2 or others with insulating-conducting behavior materials.

Introduction

The improvement of the electric grid management as well as the success of renewable energy technologies relies on energy storage. Redox flow batteries (RFBs) are promising energy storage candidates because they offer long life, low cost, high round-trip efficiency, and independent scalability of energy and power capabilities.[1] On the other hand, lithium-ion batteries (LIBs) are the power source of choice in portable electronics and electric vehicles because of their high energy density.[2] The concept of semi-solid flow batteries (SSFBs) aims at combining the best features of redox flow and Li-ion batteries; namely, the flexibility and scalability of the former and the high energy density of the latter.[3] In SSFB technology, two semi-solid suspensions, acting as positive and negative flowable electrodes, are stored in two reservoirs. The flowable suspensions typically contain active materials used in Li-ion batteries, such as $Li_4Ti_5O_{12}$, graphite, $LiCoO_2$, or $LiNi_{0.5}Mn_{1.5}O_4$. The electric energy is stored as chemical energy in the active material of the suspension. Figure 1 shows a simplified representation of a SSB system. In comparison to all-vanadium flow batteries (the most-studied and -mature among RFBs), SSFBs offer higher energy densities.[3a] Compared to classic LIBs, SSFBs offer independent scalability of energy and power capabilities, simplified manufacturing, and decrease of inactive material compared to classic LIBs.[3a]

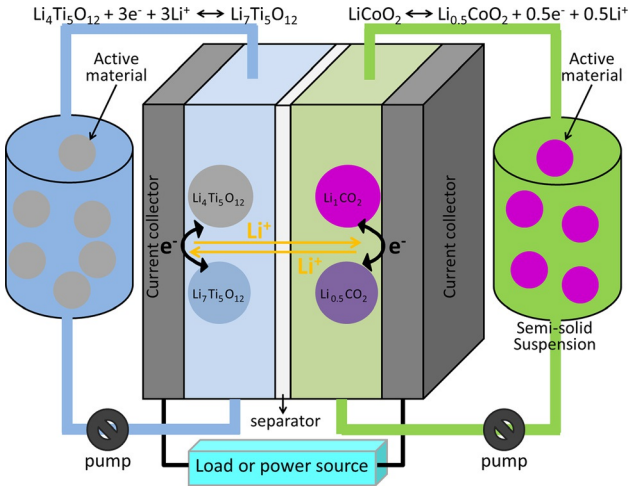

Figure 1. Schematic representation of an SSFB system.

The use of semi-solid fluid electrodes for energy storage differentiates SSFBs from other technologies. Nevertheless, obtaining good electrochemical performance from semi-solid fluid electrodes is challenging when compared to the solid electrodes of classic LIBs, because the active particles are electrically connected through the suspension. Consequently, the

[a] Dr. E. Ventosa, Dr. M. Skoumal, F. J. Vazquez, Dr. C. Flox, Prof. J. R. Morante
Department of Advanced Materials for Energy
Catalonia Institute for Energy Research
Jardins de les Dones de Negre, 1, 08930 Sant Adria de Besos (Spain)
E-mail: edgar.ventosa@rub.de

[b] Prof. J. R. Morante
Departament d'Electronica, Universitat de Barcelona
C. de Martí i Franquès, 1, 08028 Barcelona (Spain)

[c] Prof. J. Arbiol
ICREA and Institut Català de Nanociència i Nanotecnologia (ICN2)
Campus UAB, 08193 Bellaterra, CAT (Spain)

Supporting Information for this article is available on the WWW under http://dx.doi.org/10.1002/cssc.201500349.

electrical conductivity in the fluid electrode is much poorer than that of a solid electrode. In addition, the formation of an insulating solid electrolyte interphase (SEI), due to electrolyte decomposition, has a much higher impact in fluid electrodes. Common carbonate-based electrolytes used in LIBs decompose below 1 V vs Li/Li^+ at the negative electrodes. Therefore, the presence of the insulating film hinders the use of active materials operating at potentials below 1 V vs Li/Li^+ in SSFBs, leading Duduta et al.[3a] to employ $Li_4Ti_5O_{12}$ (LTO; lithium titanate) as negative electrode material in the first SSFB prototype based on carbonate electrolyte. Nevertheless, the electrical conductivity of LTO is poor and it limits the performance of this material in semi-solid flow batteries. In classic LIBs, several strategies have been employed to enhance the electrical conductivity of titania materials, such as carbon coating,[4] doping,[5] or oxygen deficiencies.[5c,6] The latter was demonstrated to be a simple and effective approach, for which the main drawback is spontaneous reoxidation in air requiring the samples to be stored in an argon-filled glove-box.[5c,7]

In addition to the technological advantages of SSFBs for energy storage, semi-solid fluid electrodes possess appealing features for fundamental studies of the active materials used in classic LIBs. One example is the online characterization of the electrode materials during the electrochemical test. Samples with different states of charge or ageing states can be easily collected from the reservoirs for ex situ investigation via X-ray photoemission, X-ray diffraction, or transmission electron microscopy without disassembling the cell, which allows one to continue with the electrochemical characterization. Another interesting feature of fluid electrodes for fundamental studies is the poorer electrical conductivity in the electrode. Whereas the electrical conductivity throughout the electrode is usually high in classic LIBs, this parameter gains importance in SSFBs and becomes a limiting factor. This allows the investigation of the pure effects of electrical properties on the electrochemical performance, which is very difficult to evaluate in solid electrodes.

In this work, we show that the electrochemical performance of a commercial LTO in semi-solid flow batteries can be improved, in terms of lower overpotentials and higher accessibility to the LTO in the fluid electrode, by subjecting the material to hydrogen annealing. In addition, the intrinsic properties of fluid electrodes allowed us to observe asymmetric electric overpotentials in LTO and TiO_2 for the oxidation/reduction processes. This phenomenon is proposed to originate from the so-called electron bottleneck mechanism based on the transformation from electrical insulator to conductor upon (de)-lithiation, or vice versa, which explains its absence in the case of $LiCoO_2$.

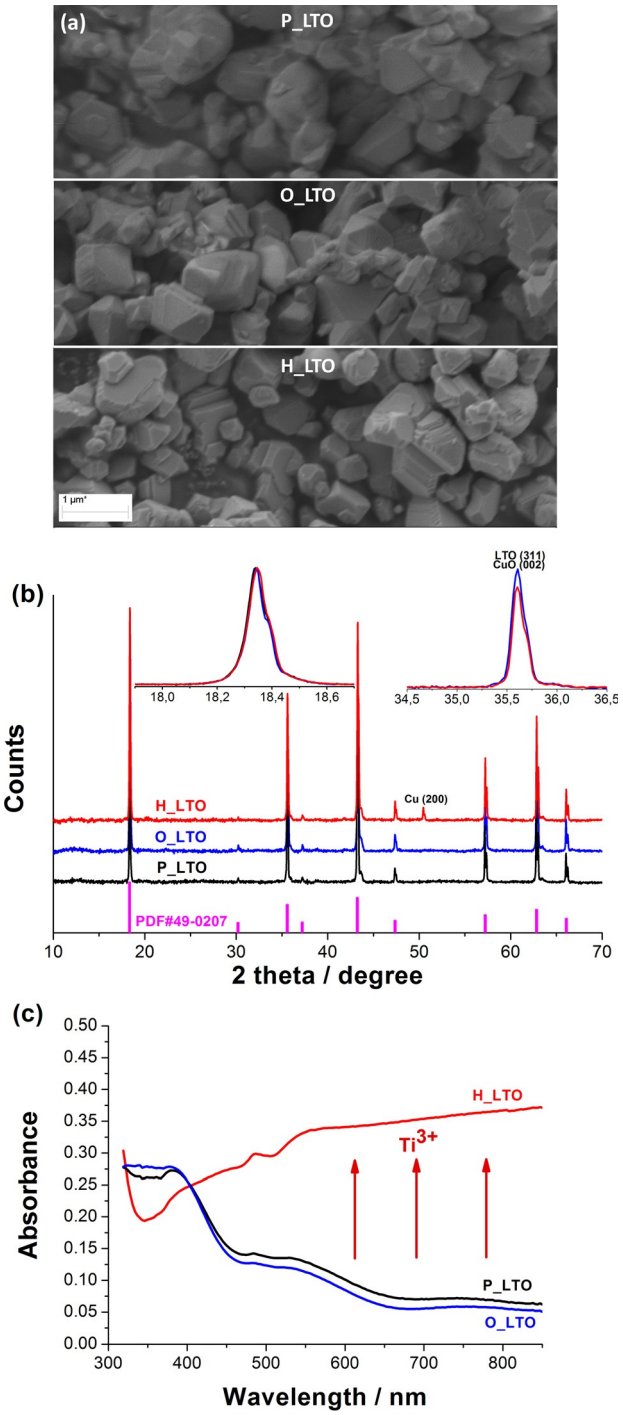

Figure 2. (a) SEM images, (b) XRD patterns, and (c) UV/Vis spectra of P_LTO, O_LTO, and H_LTO.

Results and Discussion

Structural characterization

Commercially available LTO was first annealed in oxygen at 650 °C for 120 min to remove possible surface residues, which have been shown to negatively influence the electrochemical performance.[8] After that, the O_2-annealed sample was annealed in a hydrogen atmosphere (5% H_2 in Ar) at 650 °C for 90 min. The three samples are referred to as P_LTO, O_LTO, and H_LTO for pristine, O_2-annealed, and H_2-annealed LTO, respectively. The specific surface area, morphology, and crystallinity of the three samples were evaluated. The specific surface area was determined by the Brunauer–Emmett–Teller (BET) method, obtaining values of 2.1, 2.1, and 2.0 $m^2 g^{-1}$ for P_LTO, OLTO and H_LTO, respectively, ruling out sintering effects during the annealing processes. Figure 2a show scanning elec-

tron microscopy images of the three samples. No significant changes were observed in the morphology of the samples.

Figure 2b displays X-ray diffraction patterns of the three samples. All samples completely matched the standard card of $Li_4Ti_5O_{12}$ (PDF 49-0207). An additional weak peak was obtained for H_LTO at 50.5°, which will be explained later. The inset in Figure 2b is a magnification of the main peak at 18.3°. The width of the peak for the three samples was very similar indicating similar crystallite size. We estimated the crystalline size of the samples obtaining values of 100 nm, 95 nm, and 100 nm for P_LTO, O_LTO and H_LTO. Assuming an error of 5% in the measurement, the crystallite size of the three samples falls in the range of 100±5 nm. Figure 2c shows UV/Vis spectra of P_LTO, O_LTO, and H_LTO. The oxygen vacancies created in titania via hydrogen treatment are compensated by the partial reduction of Ti^{4+} to Ti^{3+}, which introduces changes in the electronic structure. The presence of Ti^{3+} has been reported to increase absorbance above 500 nm, giving the material a blue color.[5c,9] The UV/Vis spectra (Figure 2c) revealed the introduction of oxygen vacancies in H_LTO as the absorbance above 500 nm increased clearly for that sample.

We performed X-ray photoemission spectroscopy (XPS) measurements on the three samples. Figure 3a shows XPS spectra of P_LTO, O_LTO, and H_LTO, revealing the presence of the expected elements carbon, titanium, and oxygen, and some additional elements: potassium and zirconium (Figure 3b), and copper (Figure 3c). The presence of these impurities is likely due to the industrial synthesis and processing of the LTO, such as grinding of the powders with zirconia balls, and other treatments. While the presence of zirconium and potassium do not significantly affect the analysis of the results, the contribution of copper must be taken into account. In the XPS spectra of Cu 2p region (Figure 3c), there appears to be a shift in signal of Cu 2p towards lower binding energies for H_LTO, suggesting the reduction of copper. Figure 3d shows the spectra of C 1s region. The intensity of this peak decreased significantly from P_LTO to O_LTO and H_LTO, which confirms the removal of surface organic residues during the annealing in oxygen. In the Ti 2p region (Figure 3f), no significant differences were found between the three samples. Although the successful introduction of oxygen vacancies in LTO via H_2 annealing was evident by the blue color of H_LTO (presence of Ti^{3+}),[5c,6a,b,c] we were unable to confirm it by XPS. This could be due to a low amount of Ti^{3+} and/or surface oxidation during the sample preparation. H_LTO samples were stored in the glovebox because the oxidation of Ti^{3+} has been reported to occur spontaneously in air.[5c,7] Unfortunately, we had to prepare the XPS samples outside the glovebox because of the impossibility of transferring it directly within the XPS system.

Since the XPS signal was noisy in the copper region, we employed electron energy-loss spectroscopy (EELS) chemical com-

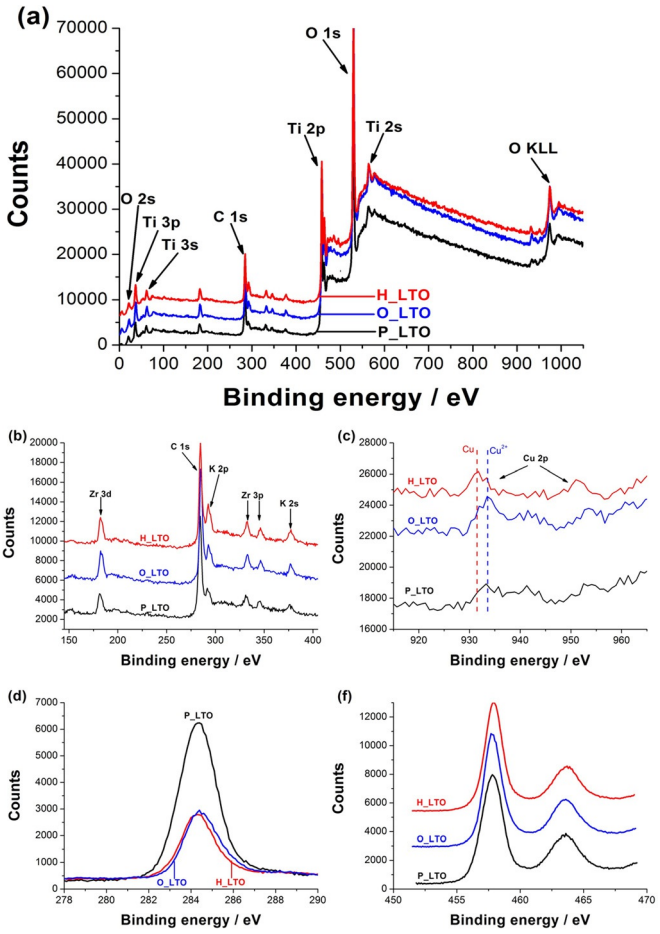

Figure 3. XPS spectra of P_LTO, O_LTO, and H_LTO for different regions: (a) full spectra, (b) Zr, K, and C region, (c) Cu region, (d) C 1s region, and (f) Ti 2p region.

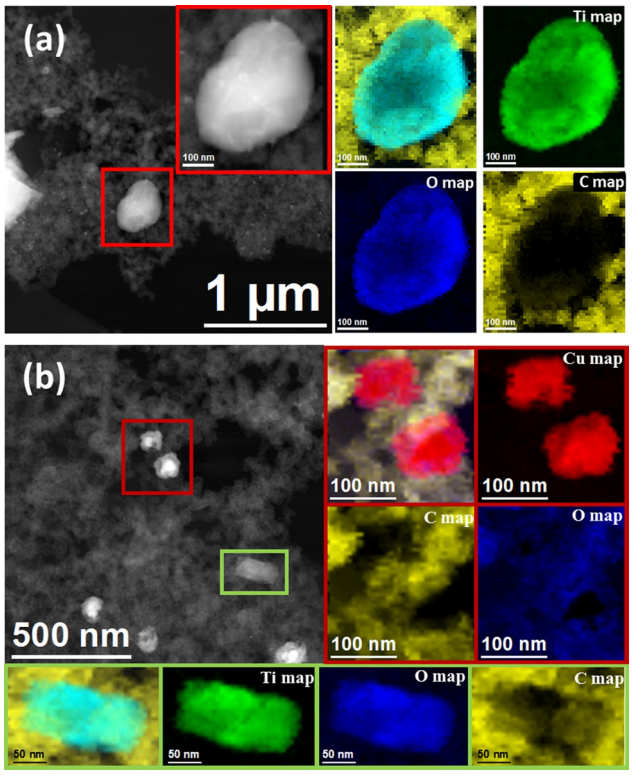

Figure 4. EELS chemical composition maps obtained from the red- and green-squared areas on the HAADF STEM image. Individual Cu (red), Ti (green), O (blue), and C (yellow).

position mapping in the scanning transmission electron microscope (STEM) to confirm the presence of copper particles. Figure 4 show the images of O_LTO suspension after an electrochemical cycle. Figure 4a displays the chemical composition of a LTO particle, for which the mean size was above 350 nm (particles up to 600 nm). Figure 4b shows the chemical composition of a copper-rich particle, in which titanium was not detected. The mean size of the copper nanoparticles was 33 nm ± 7 nm (much smaller than LTO). The copper particles appear to have a core–shell structure. Whereas the core is metallic copper, the shell is oxidized, which may be due to the exposure of the sample to air having been reduced electrochemically. Note that the carbon background is due to the ethylene carbonate as well as carbon additive remaining from the electrolyte suspension.

After confirming the presence of copper, we propose the following explanation for our XRD results. The appearance of the peak at 50.5° in the XRD pattern of H_LTO (Figure 2b) suggests the presence of metallic copper since this peak can be attributed to the (200) plane of metallic copper whereas the (111) plane overlaps one of the main peaks of LTO at 43.3°. Copper was not revealed in P_LTO and O_LTO, although it should be present. It is known that copper oxide (CuO) can grow preferentially in (002) orientation on certain substrates.[10] Assuming that this is the case for LTO, CuO (002) overlaps LTO (311) at 35.6°. Interestingly, this peak at 35.6° is the only one decreasing in intensity for H_LTO (inset in Figure 2b). Thus, the decrease in the intensity at 35.6° occurring simultaneously with the appearance of the peak at 50.5° suggests that CuO is reduced to metallic copper during hydrogen treatment.

Electrochemical characterization

We evaluated the electrochemical properties of the suspensions of three samples, namely P_LTO, O_LTO and H_LTO, containing 25 wt%, and 1 wt% of active material and carbon additive, respectively, in 1 M $LiPF_6$ in ethylene carbonate/dimethyl carbonate (EC/DMC 1:1). The suspensions were studied in static (without flow) and in dynamic (with a flow of ca. 3 mL min^{-1}). Figure 5 shows the potential profiles of the three samples for the first cycle in static conditions at ca. 0.1 C (16 mA g^{-1}) and clearly reveals the beneficial effect of H_LTO. The reversible charge capacities, extracted from the anodic cycle, were 80, 130, and 170 mAh g^{-1} for P_LTO, O_LTO, and H_LTO, respectively. The removal of the surface organic residues, during O_2 annealing, is likely responsible for the improvement observed from P_LTO to O_LTO. The organic residues not only can act as barrier for electron transfer but also can lead to undesired side reactions, for example, electrochemical reduction of some elements of carbonaceous residues.[8b] The removal of adsorbed water by air annealing was also reported to improve the performance of titania materials in LIBs.[8a] In addition, the reduction of CuO in both P_LTO and O_LTO could contribute to the low Coulombic efficiency of these samples in the first cycle. On the other hand, the improvement obtained via hydrogen annealing appeared to be an increased accessibility to all of the LTO particles in the suspension by the enhancement of the electrical properties of H_LTO. Interestingly, the overpotentials for H_LTO during the anodic process were significantly lower than those of P_LTO and O_LTO because the potential plateaus of H_LTO were closer to the standard redox potential of LTO (1.55 V vs Li/Li^+). The higher anodic overpotentials of P_LTO and O_LTO appeared to prevent the full deintercalation for an upper cut-off potential of 2.9 V vs Li/Li^+.

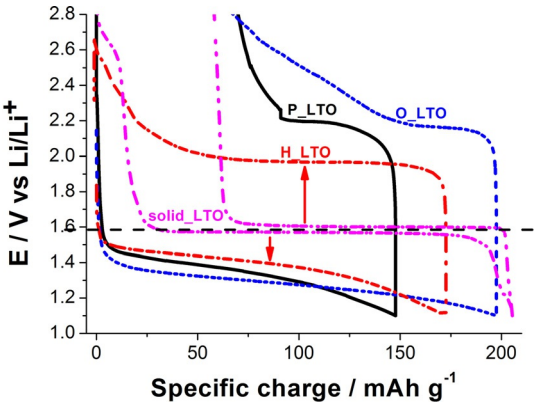

Figure 5. Potential profiles for the first cycle of P_LTO, O_LTO, and H_LTO as fluid electrode in static and O_LTO as solid electrode.

Figure 5 also revealed another interesting feature. The improvement in H_LTO was higher for the anodic process. And, more importantly, the anodic overpotentials for the three samples were significantly higher than the cathodic ones, which did not occur in solid electrodes at 0.1 C. Note that the potential profile of O_LTO in solid electrode is included in Figure 4 for comparison. There are three major contributors to any polarization overpotential; the charge transfer resistance, the ionic resistance and the electrical resistance. I) We evaluated the charge transfer resistance by electrochemical impedance spectroscopy (EIS) of the samples as solid electrodes (Supporting Information, Figure S1). The solid electrode films contained 90% of LTO and 10% of binder. Without carbon additive, the charge transfer resistances of O_LTO and H_LTO were small at any state of charge (Figure S1). The charge transfer resistance can only account for 30–60 mV of overpotential. II) The ionic resistance both in the liquid and in the solid was minimized by applying low current density of 16 mA g^{-1} and long charge/discharge times of 10 h. The ionic resistance of the electrolyte, determined by electrochemical impedance spectroscopy, was around 3 Ω accounting for only 6 mV overpotential. III) There are two types of electrical resistance; a) the electrical resistance through the fluid electrode (the suspension), and b) the electrical resistance of the carbon–LTO contact point, which is determined by the electrical conductivity of LTO at the surface. The electrical percolation of the three suspensions was dominated by the conductive additive since similar values of electrical conductivity were obtained for the three samples (17, 20, and 20 μS cm^{-1} for P_LTO, O_LTO and H_LTO, respectively). The Ohmic drop across the fluid electrode is similar for all samples, indicating that the electrical resistance at the carbon–LTO con-

tact point is the main factor responsible during the charge/discharge process. The electrical conductivity obtained for H_LTO was 1.5×10^{-10} S cm^{-1}. This value is lower than that previously reported for hydrogen-treated LTO (8×10^{-8} S cm^{-1}),[5c] which is attributed to the fact that our film was porous and contained binder, as well as the resistance being determined by two-probe measurements. The resistance of P_LTO and O_LTO were above the measurable limit of our equipment (> 2000 MΩ). Therefore, their electrical conductivities are below 3×10^{-12} S cm^{-1}, which is consistent with the values reported for LTO (< 10^{-13} S cm^{-1}).[5c] The electrical conductivity of H_LTO was, at least, two orders of magnitude higher than those of P_LTO and O_LTO.

The evidence of highly asymmetry overpotential provided only in SSFBs is due to the fact that the electrical properties of the carbon–LTO contact points have a strong influence on the Ohmic overpotentials of fluid electrodes. Compared to solid electrodes, the density of active and conductive material in the fluid electrode is much lower and, thus, the electrical percolation and the number of interconnections between particles is much smaller for fluid electrodes. In other words, the number of carbon–LTO contact points is much lower for fluid electrodes, which has a large impact because all electrons pass through these points. Since the area of the contact points is very small, the current density passing through it is very high, making the contact points the limiting factor of the electrical resistance. For a given current intensity, a lower number of electrical contact points leads to lower carbon–LTO interface area and to a higher electrical resistance and, therefore, a higher Ohmic drop. The contact area of LTO, acting as electron bottleneck, comprises reduced LTO ($Li_7Ti_5O_{12}$) during the entire reduction and oxidized LTO ($L_4Ti_5O_{12}$) during the entire oxidation because electrons continuously pass through those points. Since the electrical conductivity changes from electrically insulating ($10^{-7\sim12}$ S cm^{-1}) to conducting (2 S cm^{-1}) for oxidized and reduced phases,[11] respectively, the electrical resistances at the contact points are expected to be much higher during the oxidation due to the presence of the insulating phase ($L_4Ti_5O_{12}$) at the contact points. The hydrogen treatment probably improves the electrical conductivity of the surface and does not reach the core. However, having a layer of conducting material will increase the conducting contact area significantly; reducing the resistance considerably (resistance is inversely proportional to the conducting area).

Figure 6 is a schematic representation of the proposed electron bottleneck during the oxidation of $Li_7Ti_5O_{12}$. The drastically improved accessibility in the anodic process observed for H_LTO as compared to P_LTO and O_LTO can now be explained by the proposed mechanism. During the oxidation, the electrical conductivity of lithiated LTO should be sufficient. However, the first electrons will be extracted from the contact points with the carbon and those points will remain oxidized during the entire oxidation. In the case of H_2-treated LTO, the oxygen vacancies created at the surface of LTO are permanent and they will remain at the surface during the entire oxidation. Therefore, the electron gateways (LTO–carbon contacts) will have a higher electrical conductivity in the case of H_2-treated

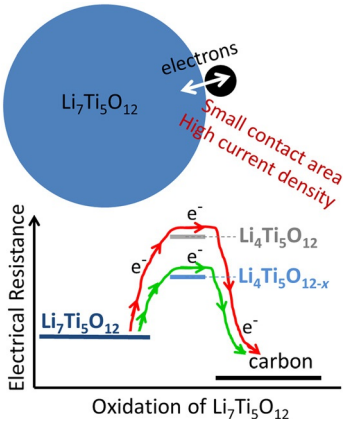

Figure 6. Scheme of the proposed electron bottleneck mechanism for oxidation of $Li_7Ti_5O_{12}$.

samples due to the permanent oxygen vacancies at the surface. In classic Li-ion batteries, the mechanism by which oxygen deficient titania (TiO_{2-x} or $Li_4Ti_5O_{12-x}$) delivered better performances than pristine titania (TiO_2 or $Li_4Ti_5O_{12}$),[5c, d, e, f, 6b] was not fully understood, considering that titania is always partially reduced during operation. The bottleneck mechanism offers an explanation.

The highly asymmetric anodic/cathodic electric overpotentials should not be a unique feature of $Li_4Ti_5O_{12}$ but should occur in other materials with large difference in electrical conductivity between the lithiated and delithiated phases, also. The case of titanium dioxide (TiO_2) is analogous to that of LTO because the oxidized phase (TiO_2) and reduced phase ($Li_{0.5}TiO_2$) present electrically insulating ($10^{-7\sim10}$ S cm^{-1}) and conducting behavior (9 S cm^{-1}), respectively.[5d, 12] Indeed, TiO_2 also showed a highly asymmetric overpotential for reduction/oxidation in SSFBs at ca. 0.1 C, which did not occur in the solid electrode (Figure 7a). On the other hand, $LiCoO_2$ has a good electrical conductivity (0.2 S cm^{-1}), which actually increases to metallic conductivity (500 S cm^{-1}) upon oxidation ($Li_{0.5}CoO_2$).[13] Since neither the oxidized nor the reduced phase possesses electrically insulating behavior, the asymmetric electric overpotential should not occur for $LiCoO_2$. Figure 7b show the potential profile of a fluid and a solid electrode of $LiCO_2$ at ca. 0.1 C, and the asymmetric overpotentials were not observed in this case.

The analysis of the symmetry of the electric overpotential of materials by fluid electrodes allows one to separate the ionic and electrical contributions during charge/discharge. In addition, the phenomenon is of great importance for modeling, evaluating, or designing advanced materials.

The suspensions containing LTO were evaluated in continuous flow of ca. 3 mL min^{-1}. Figure 8 shows the anodic potential profiles of P_LTO, O_LTO, and H_LTO at 3 mA cm^{-2}. For fast cathodic process, a combination of galvanostatic and potentiostatic modes was applied. First, a constant current density of 3 mA cm^{-2} was applied until the lower cutoff potential of 1.1 V vs Li/Li$^+$ was reached. Then, a constant potential of 1.1 V was applied until the current density reached a value below 1.5 mA cm^{-2}. The anodic process was carried out in galvano-

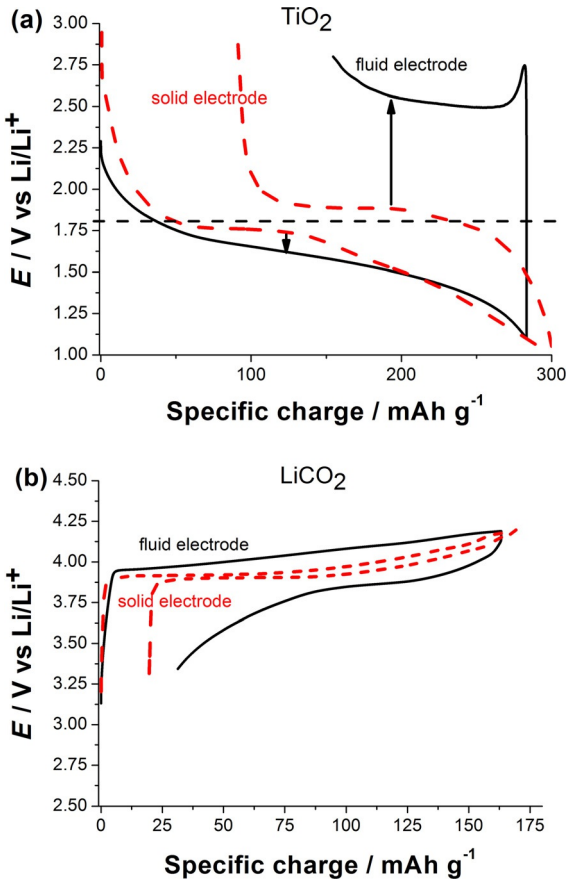

Figure 7. Potential profiles of (a) TiO_2 and (b) $LiCoO_2$ as fluid electrode and as solid electrode.

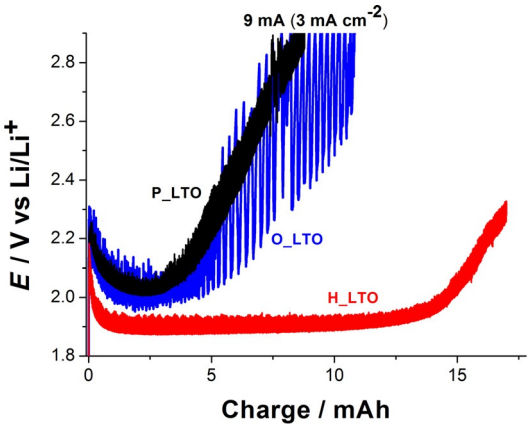

Figure 8. Potential profile of P_LTO, O_LTO, and H_LTO for the anodic cycle at 3 mA cm^{-2} and 3 mL min^{-1}.

static mode applying a current density of 3 mA cm^{-2}. To clarify the figure, we omit the combined galvanostatic–potentiostatic cathodic step and we represent only the anodic step, which was found to be the relevant one in the previous section. Figure 7 shows the anodic potential profiles of P_LTO, O_LTO, and H_LTO. There was no significant improvement from P_LTO to O_LTO. As expected, the performance of H_LTO in continuous flow was improved with respect to P_LTO and O_LTO. The oxidation plateau was more than 100 mV lower than that of P_LTO and O_LTO. In addition, the amount of charge reversibly stored in the case of H_LTO was significantly larger than that of P_LTO and O_LTO under the same conditions. The comparison of the anodic processes in static and flowing conditions (Figure 5 and Figure 7 respectively), one can see i) a noisy potential signal, and ii) lower overpotentials for all samples in flowing conditions. Our peristaltic pump of three rollers did not provide a highly smooth flow for viscous suspensions. As a consequence, the potentials recorded the little injections into the reactive channel leading to noisy signal. An improved electrical percolation in flow could be the source. However, we cannot unambiguously attribute the noise to only electrical conductivity issues of the suspension because the concentration gradients at the high current density in flowing conditions (0.67 and 3.00 mA cm^{-2} for static and flow, respectively) might not be negligible. Similar reasoning applies to the lower overpotentials in flowing conditions. Further detailed analysis will be required to properly understand this phenomenon.

Conclusions

The hydrogen annealing of $Li_4Ti_5O_{12}$ (LTO) leads to significant improvement in the electrochemical performance when the material is employed as active material in semi-solid flow batteries (SSFBs). This thermal treatment appears to enhance the accessibility to the active material within the suspension, especially during the anodic process. For all LTO samples tested as fluid electrode, the oxidation process presents higher overpotentials than the cathodic ones, which does not occur in solid electrodes at the same C rate (0.1 C). While ionic and electrical resistances are difficult to separate in solid electrodes in operando conditions, the latter is the main contributor in fluid electrodes. Active materials transforming from electrically insulator to conductor upon (de)lithiation, such as $Li_4Ti_5O_{12}$ and TiO_2, show asymmetric overpotentials for charge/discharge as fluid electrodes. On the other hand $LiCoO_2$, without an electrically insulating phase (both $LiCoO_2$ and $Li_{0.5}CoO_2$ are electrically conducting), does not reveal asymmetric overpotentials. We propose the electron bottleneck mechanism to explain the asymmetric overpotential. The bottleneck mechanism offers an explanation for the improved electrochemical performance of oxygen-deficient titania in classic lithium-ion batteries. As a consequence of the bottleneck effect, the use of electrically insulating materials in SSFB requires the optimization of the electrical conductivity of the suspension by adding an adequate amount of carbon for optimal electrical percolation. Additional coating of the active material with conducting material, for example, carbon, metal, or through doping, is an excellent strategy. We encourage the asymmetric electrical conductivity to be considered when modeling, evaluating, and designing advanced active materials with asymmetric electrical conductivity for the oxidized and reduced phase

Experimental Section

Materials and thermal treatment

The following active materials were employed in this work: $Li_4Ti_5O_{12}$ (D50 1.9 μm) from MTI Corporation, $LiCoO_2$ (7–10 μm) from Sigma–Aldrich, and anatase TiO_2 (< 10 nm) from Sachtleben Chemie. All components of the electrolyte, namely ethylene carbonate and dimethyl carbonate and $LiPF_6$, and metallic lithium were purchased from Sigma–Aldrich (battery grade). Celgard 2500 and Ketjenblack EC-600 JD were courtesy of Azelis and AkzoNovel Polymer Chemicals.

The oxygen-annealed $Li_4Ti_5O_{12}$ samples (O_LTO) were obtained by treatment commercially available $Li_4Ti_5O_{12}$ (P_LTO) in flowing O_2 (100 vol%) at 650 °C for 120 min. The O_2-annealed sample (O_LTO) was then treated in flowing H_2 (5 vol% in Ar) at 650 °C for 90 min to obtain hydrogen-annealed $Li_4Ti_5O_{12}$ (H_LTO).

Structural characterization

The BET surface areas were determined by nitrogen physisorption using a TriStar II 3020 from Micromeritics. The samples were outgassed at 250 °C for 5 h before the measurement.

The morphology of the samples was examined by using a ZEISS Auriga microscope.

High resolution transmission electron microscopy (HRTEM) analyses were carried out with a field emission gun microscope FEI Tecnai F20, working at 200 kV and with a point-to-point resolution of 0.19 nm. Electron energy loss spectroscopy (EELS) spectra were obtained in a GATAN Quantum detector coupled to the F20 microscope.

X-ray power diffraction (XRD) analyses were carried out on a Bruker AXS D8 ADVANCE X-ray diffractometer with $CuK_{\alpha 1}$ radiation ($\lambda = 1.5406$ Å).

The UV/Vis spectra were recorded in diffuse reflectance mode in a PerkinElmer Lambda 950 UV/Vis spectrometer equipped with a 150 mm Int. Sphere (PerkinElmer). BaSO4 was used as a reference material.

The chemical composition of the surface of the LTO was analyzed by X-ray photoelectron spectroscopy (XPS) using a PHI instrument model 5773 Multitechnique with A1K radiation (1486.6 eV).

Suspension preparation

The fluid electrodes were prepared by mixing the active materials and carbon additive in the electrolyte (EC:DMC in 1 M $LiPF_6$) by magnetic stirring for overnight. The fluid electrode was flowed through the cell for, at least, 1 h before starting the experiments to further homogenize the suspension. The reservoirs were constantly stirred during the electrochemical characterization.

For the suspensions, 2.5 g and 0.125 g of active and conductive additive, respectively, were added into 12 mL for TiO_2 and $LiCoO_2$ and into 6 mL for LTO. The poor electrical conductivity and low surface area of LTO forced us to increase the concentration of particles in the suspension to obtain decent performances.

For solid electrodes, A slurry containing 75:15:10 wt% of active material, conductive additive and poly(vinylidene difluoride) (PVDF) binder (Sigma–Aldrich) was prepared by dispersing in *N*-methyl pyrrolidone (NMP) (Sigma–Aldrich) and mixing for overnight using magnetic stirring. The slurry was doctor-bladed onto copper foil (Schlenk) and dried at 60 °C for 10 h in air, resulting in an active material loading of about 3 mg cm^{-2}. 10 mm disk electrodes were punched out using a commercially available hole punch (Hoffmann) and dried overnight at 80 °C in a vacuum oven

Electrochemical characterization

The electrochemical cells for the characterization of both solid and fluid electrode were two-electrode configuration and were assembled in an Ar-filled glove box ($O_2 < 1$ ppm and $H_2O < 1$ ppm). Pure lithium metal was used for counter and reference electrodes. Celgard 2500 and EC:DMC in 1 M $LiPF_6$ served as separators and electrolyte, respectively. The electrochemical cell employed for testing fluid electrodes is shown in Figure S2 (Supporting Information). The dimensions of the channel were 75×4×1 mm and the current collector was metallic copper. Electrochemical measurements were performed with a Bio-Logic VMP-3 (Bio Logic SAS).

Electrical conductivity of active material

Films containing 90% of LTO and 10% of poly(vinylidene difluoride) (PVDF; binder) were prepared on copper foil by the doctor blade technique. The thickness of the resulting films was ca. 45 micrometer, which was measured with a digital external micrometer (HOLEX 421505). Discs of 12 mm diameter were cut and the electrical conductivity was estimated by 2 probe measurement using a multimeter (UNI-T UT70A).

Electrical conductivity test of suspensions

The measurements for electrical conductivity were carried out using the same cell employed for the electrochemical evaluation of fluid electrode, with the exception of the separators and the metallic lithium. Titanium current collectors were used for higher stability. The electrical resistivity of the suspension was then estimated with multimeter (Silver Electronics UT33D) knowing the section and the length of the cell (3 cm^2×1 mm). Note that the objective of these measurements was to compare the electrical conductivities of the three suspension (P_LTO, O_LTO and H_LTO), rather than obtaining the exact values. To avoid changing the cell configuration factor for the different samples, the cell was not disassembled between the three experiments but it was vigorously cleaned with pure DMC.

Electrochemical impedance spectroscopy (EIS)

The solid electrode prepared for the measurement of the electrical conductivity of the active material (90:10 LTO/binder) were also employed for EIS. A typical three-electrode Swagelok cell using metallic lithium as counter and reference electrode was used. Whatman and EC/DMC in 1 M $LiPF_6$ served as separators and electrolyte, respectively. The cell was assembled in an argon-filled glove-box, then taken outside the glove-box and tested with a Bio-Logic VMP-3 (Bio Logic SAS). The state of charge was tuned galvanostatically at 0.1 C. The EIS were performed in a frequency range of 100 kHz–0.020 Hz with an amplitude of 20 mV.

Acknowledgements

The research leading to these results has received funding from the European Union Seventh Framework Programme (FP7/2007-2013) under grant agreement n° 608621. Authors thank the Gen-

eralitat de Catalunya 2014SGR1638. J.A. thanks ICN2 Severo Ochoa Excellence grant.

Keywords: batteries · conductivity · metal oxides · oxidation · reduction

[1] a) M. Skyllas-Kazacos, F. Grossmith, *J. Electrochem. Soc.* **1987**, *134*, 2950; b) C. Ponce de León, A. Frías-Ferrer, J. González-García, D. A. Szánto, F. C. Walsh, *J. Power Sources* **2006**, *160*, 716; c) Z. G. Yang, J. L. Zhang, M. C. W. Kintner-Meyer, X. C. Lu, D. W. Choi, J. P. Lemmon, J. Liu, *Chem. Rev.* **2011**, *111*, 3577.

[2] a) J. M. Tarascon, M. Armand, *Nature* **2001**, *414*, 359; b) M. S. Whittingham, *Chem. Rev.* **2004**, *104*, 4271; c) A. S. Aricò, P. Bruce, B. Scrosati, J. M. Tarascon, W. van Schalkwijk, *Nat. Mater.* **2005**, *4*, 366.

[3] a) M. Duduta, B. Y. Ho, V. C. Wood, P. Limthongkul, V. E. Brunini, W. C. Carter, Y.-M. Chiang, *Adv. Energy Mater.* **2011**, *1*, 511; b) S. Hamelet, T. Tzedakis, J.-B. Leriche, S. Sailler, D. Larcher, P.-L. Taberna, P. Simon, J.-M. Tarascon, *J. Electrochem. Soc.* **2012**, *159*, A1360; c) Y. Yang, G. Zheng, Y. Cui, *Energy Environ. Sci.* **2013**, *6*, 1552; d) S. Hamelet, D. Larcher, L. Dupont, J.-M. Tarascon, *J. Electrochem. Soc.* **2013**, *160*, A516; e) F. Y. Fan, W. H. Woodford, Z. Li, N. Baram, K. C. Smith, A. Helal, G. H. McKinley, W. C. Carter, Y.-M. Chiang, *Nano Lett.* **2014**, *14*, 2210 – 2218.

[4] a) H.-G. Jung, S.-T. Myung, C. S. Yoon, S.-B. Son, K. H. Oh, K. Amine, B. Scrosati, Y.-K. Sun, *Energy Environ. Sci.* **2011**, *4*, 1345; b) L. Zhao, Y.-S. Hu, H. Li, Z. Wang, L. Chen, *Adv. Mater.* **2011**, *23*, 1385.

[5] a) D. Capsoni, M. Bini, V. Massarotti, P. Mustarelli, G. Chiodelli, C. B. Azzoni, M. C. Mozzati, L. Linati, S. Ferrari, *Chem. Mater.* **2008**, *20*, 4291; b) H. Song, S.-W. Yun, H.-H. Chun, M.-G. Kim, K. Y. Chung, H. S. Kim, B.-W. Cho, Y.-T. Kim, *Energy Environ. Sci.* **2012**, *5*, 9903; c) H. Song, T. G. Jeong, Y. H. Moon, H. H. Chun, K. Y. Chung, H. S. Kim, B. W. Cho, Y. T. Kim, *Sci. Rep.* **2014**, *4*, 4350; d) J.-Y. Shin, J. H. Joo, D. Samuelis, J. Maier, *Chem. Mater.* **2012**, *24*, 543; e) E. Ventosa, W. Xia, S. Klink, F. La Mantia, B. Mei, M. Muhler, W. Schuhmann, *Chem. Eur. J.* **2013**, *19*, 14194; f) E. Ventosa, A. Tymoczko, K. Xie, W. Xia, M. Muhler, W. Schuhmann, *ChemSusChem* **2014**, *7*, 2584.

[6] a) T. Yuan, R. Cai, Z. Shao, *J. Phys. Chem. C* **2011**, *115*, 4943; b) J. Wolfenstine, U. Lee, J. L. Allen, *J. Power Sources* **2006**, *154*, 287; c) L. Shen, E. Uchaker, X. Zhang, G. Cao, *Adv. Mater.* **2012**, *24*, 6502.

[7] a) K. Komaguchi, T. Maruoka, H. Nakano, I. Imae, Y. Ooyama, Y. Harima, *J. Phys. Chem. C* **2010**, *114*, 1240; b) F. Zuo, L. Wang, T. Wu, Z. Zhang, D. Borchardt, P. Feng, *J. Am. Chem. Soc.* **2010**, *132*, 11856.

[8] a) E. Madej, F. La Mantia, B. Mei, S. Klink, M. Muhler, W. Schuhmann, E. Ventosa, *J. Power Sources* **2014**, *266*, 155; b) Z. Sun, X. Huang, M. Muhler, W. Schuhmann, E. Ventosa, *Chem. Commun.* **2014**, *50*, 5506.

[9] X. Yu, R. Wang, Y. He, Y. Hu, H. Li, X. Huang, *Electrochem. Solid-State Lett.* **2010**, *13*, J99.

[10] a) M. Hussain, A. Khan, O. Nur, M. Willander, *Acta Phys. Pol. A* **2014**, *126*, 849; b) K. K. Dey, P. Kumar, R. R. Yadav, A. Dhara, A. K. Srivastav, *RSC Adv.* **2014**, *4*, 10123.

[11] D. Young, A. Ransil, R. Amin, Z. Li, Y.-M. Chiang, *Adv. Energy Mater.* **2013**, *3*, 1125.

[12] R. Van de Krol, A. Goossens, E. A. Meulenkamp, *J. Appl. Phys.* **2001**, *90*, 2235.

[13] Y. Takahashi, N. Kijima, K. Tokiwa, T. Watanabe, J. Akimoto, *J. Phys. Condens. Matter* **2007**, *19*, 436202.

Received: March 8, 2015
Published online on April 17, 2015

